NAG5-1012

CLOUDS, SURFACE TEMPERATURE, AND THE TROPICAL AND SUBTROPICAL RADIATION BUDGET

IN-47-CR
81429
P.13

Harbans L. Dhuria
University of the District of Columbia, Washington, DC

H. Lee Kyle
NASA/Goddard Space Flight Center, Greenbelt, MD

1. INTRODUCTION

The solar energy drives both the Earth's climate and biosphere, but the absorbed energy is unevenly distributed over the Earth. The tropical regions receive excess energy which is then transported by atmospheric and ocean currents to the higher latitudes. All regions at a given latitude receive the same top of the atmosphere solar irradiance (insolation). However, the net radiation received from the Sun in the tropics and subtropics varies greatly from one region to another depending on local conditions. Over land, variations in surface albedo are important. Over both land and ocean, surface temperature, cloud amount, and cloud type are also important. This study uses the Nimbus-7 cloud and Earth radiation budget (ERB) data sets to examine the affect of these parameters on the radiation over the course of 1 year (June 1979 to May 1980).

Clouds are the most important and also the most variable moderator of the radiation budget. The four components of the planetary radiation budget are the top-of-the-atmosphere (TOA): insolation (solar irradiance), outgoing longwave radiation (OLR), absorbed shortwave (ASW), and net radiation (NR). They are connected by the equation:

$$NR = (I - A)I_S - OLR \qquad (1)$$

where:

I_s is the insolation

A is the albedo, and

ASW = $(I-A)I_s$ is the absorbed shortwave radiation

NASA-CR-190318
CLOUDS, SURFACE TEMPERATURE, AND THE TROPICAL AND SUBTROPICAL RADIATION BUDGET (District of Columbia Univ.) 13 p CSCL 04B
N92-23431
G3/47 Unclas 0081429

Several studies, using satellite data, have recently examine the effects of clouds on the radiation budget (see for instance Arking, 1991; Ardanuy et al., 1991; Harrison et al., 1990; Hartmann and Doelling, 1991; and Dhuria and Kyle, 1990). Low thick clouds sharply reduce the absorbed, but only slightly reduce the emitted radiation; thus, they strongly decrease the net radiation. Conversely, thin, high-altitude cirrus clouds can increase the net radiation by only slightly reducing the absorbed while strongly reducing the emitted radiation. In the global mean, clouds reduce the net radiation received from the Sun. However, in the tropics, clouds can regionally either increase or decrease the net radiation depending on cloud type and amount. In the mean, clouds just slightly decrease the tropical net radiation.

Of course, cloud types and amount are dependent on the regional climate and, in particular, on the surface temperature. Thus, some relationship between the regional surface temperature and net radiation might be suspected. In fact, the cooler regions generally have a lower net radiation than do the warmer ones. They also tend to show a different pattern for the seasonal cycle of the radiation budget parameters. These differences in the tropics and subtropics are examined in this study over the course of 1 year (June 1979 to May 1980). The Nimbus-7 cloud and Earth radiation budget scanner data are briefly described in Section 2, Section 3 gives an overview of the problem based on annual means, while seasonal variations are discussed in Section 4. A summary and discussion come in Section 5.

2. THE NIMBUS-7 CLOUD AND EARTH RADIATION BUDGET DATASETS

The Nimbus-7 satellite was launched into a stable, nearly circle, Sun-synchronous orbit on October 24, 1978. The mean spacecraft altitude is 955 km, the orbit period is 104 minutes, and equator crossings are a little before noon and midnight local time. The spacecraft carried into orbit a diverse complement of scientific instruments, three of which contributed to this study: the Earth Radiation Budget (ERB), the Temperature and Humidity Infrared Radiometer (THIR), and the Total Ozone Mapping Spectrometer (TOMS).

The ERB experiment (Jacobowitz et al., 1984), itself, contains three different sensor groups: a solar telescope, a set of wide-field-of-view (WFOV) Earth flux sensors, and a narrow-field-of-view (NFOV) scanner. Separate Earth radiation budget datasets were derived from the WFOV and NFOV measurements. The scanner has the better spatial resolution with a nadir footprint about 90 km x 90 km). The scanner failed on June 22, 1980, but the WFOV and solar sensors are still taking measurements. The total solar irradiance measurements are still being released (Hoyt et al., 1991), but due to budget constraints, the final calibration of the WFOV measurements stopped after data month October 1987.

Some algorithm problems degraded the quality of the original scanner Earth radiation budget products (Kyle et al., 1985). Improved algorithms were recently used to reprocess 13 months (May 1979 to May 1980) of the scanner measurements (Ardanuy et al., 1990). It is this reprocessed product that is used in this study. The Earth radiation budget parameters considered include daily and monthly averaged TOA insolation and both clear and average sky albedo, emitted and net radiation.

The Nimbus-7 cloud dataset (Stowe et al., 1988,1989) is derived from the THIR 11.5-μm infrared (IR) and the TOMS 0.36- and 0.38-μm ultraviolet (UV) measurements. The THIR nadir footprint has a resolution of 6.7 km, while TOMS channels have a (50 km x 50 km) nadir footprint. The TOMS channels used are not affected by ozone absorption. Separate IR and UV estimates of cloud amount are made. The IR uses the 11.5-μm measurements, concurrent Air Force nephanalysis surface temperatures and regional climatological atmospheric temperature lapse rates. This allows both day and night IR cloud estimates to be made. UV cloud estimates are made only during daylight when the Air Force nephanalysis reports no snow or ice in the region. For daylight periods, the separate estimates are combined by an algorithm that gives most weight to the IR estimate for mid- and high-level clouds. However, for low clouds the UV estimate is given considerable weight. From this dataset, we used the bispectral cloud estimates, the Air Force surface temperatures, and the average clear scene and cloud top IR radiances.

ERB and cloud datasets we used consisted of daily and monthly averages on an approximately equal area global grid. It consisted of 2070 regions each about (500 km x 500 km) in size. Near the equator, regions are 4.5° latitude by 4.5° longitude. Annual means are obtained by averaging the monthly means.

3. MEAN ANNUAL RELATIONSHIPS

In the annual mean, the central half of the Earth ($\pm 30°$ latitude) absorbs more energy from the Sun that it radiates back to space. This is illustrated in Figure 1, which shows the annual net radiation for the study year. Note that in this energy excess region, there is considerably more longitudinal variation in the net radiation than there is at higher latitudes where an annual net radiation deficit exists. The energy gradients shown help drive the atmospheric and oceanic currents which carry energy from the excess to the deficit regions. In the atmosphere, the Hadley cells help carry tropical energy to the mid-latitudes. The Walker cell circulation is related to the longitudinal gradients. The ocean currents such as the Pacific Ocean Gyre and the Equatorial Pacific counter current are also important.

The mean annual surface temperatures taken from the Nimbus-7 cloud dataset (Stowe et al., 1988) are shown in Figure 2. Note that there is a general similarity in the net radiation and temperature contours. This is true of both the equator to pole and east-west gradient patterns. Physically, this makes sense since the regions that receive the most heat will generally be the warmest. It helps to simplify the analysis if land and ocean regions are treated separately. To this end, we divide the 2,070 Nimbus-7 ERB target areas into three classes:

Ocean	(over 85% water)
Land	(over 85% land)
Coast	(mixture of land and water)

Figure 3a shows a scatter plot of annual mean net radiation versus surface temperature for the entire globe (2,070 target areas). Two regimes are apparent. The polar regions with mean temperatures below 260°K form a nearly flat tail. In fact there is tendency for the net radiation to decrease as the temperature increases. The polar regions absorb little direct energy from the Sun, thus the OLR is dominant (see Eq.(1)). In this region, the OLR tends to increase, and the net radiation to decrease, as the temperature increases. Over the rest of the globe, where direct solar heating is important, there is a strong correlation between net radiation and surface temperature. Dry continental regions have their own peculiar patterns; notice that the tropical and subtropical Sahara and Arabian deserts (Figure 1) show an annual energy deficit even though the surface temperature is moderately high. In this study, we shall not consider such areas in detail.

Figure 3b treats just the ____ ocean target areas from 45°S to 45°N latitude. The correlation of 95% would seem to explain about 90% of the variance. The major strength in the correlation comes from the equator-to-pole gradients. However, the scatter plot in Figure 4 shows a 76% correlation for the _____ ocean target areas from 4.5°S to 4.5°N latitude. Geographically, the relationship is illustrated in Figure 5. This is an annual mean tropical net radiation map with the surface temperatures $\geq$301°K (28°C) or $\leq$297°K (24°C) indicated on it. Note that most of the equatorial regions with a mean net radiation over 80 W/m^2 have mean temperatures of 301°K or greater.

Over the oceans, clouds are a major moderator of albedo and OLR and hence of the net radiation. However, cloud amounts and types are dependent on the local surface temperature and other weather parameters. Thus, clouds can act as a feedback mechanism to increase the net radiant energy to warm regions and decrease it over cool regions. This is shown by the annual net radiation cloud forcing shown

in Figure 6. In the tropics oceans, the warmer regions with mean temperatures of 300°K or greater usually show a low net cloud forcing that may even be positive in nature. These warmer regions tend to have a large percentage of thin cirrus, derived from neighboring deep convective cells, which act to increase the net radiation. On the other hand, the regions with mean temperatures of 297°K or less often are covered by low stratus clouds which produce a strong negative net cloud forcing. Thus, the cool waters along the west coasts of South America and Africa are associated with strong negative cloud forcing, while the warm water in the western Pacific and Indian oceans show patches of positive cloud forcing.

Examining the equator-to-pole gradient, the cold high latitude waters show a strong negative net cloud forcing compared to the relatively mild cloud forcing over the warm tropical waters. Thus, in the mean, cloud feedback related to the surface temperature tends to modulate solar heating to keep warm regions warm and cool regions cool.

Over continents, the variability in the surface water, surface albedo, and the presence of mountains complicate the patterns. However, there are regions such as warm northern India and the cooler South China where the same pattern exists. Our main emphasis in this study is on the oceans.

The analysis, in the next section, of the seasonal variations in the tropics and subtropics yield additional insight on the relationship between clouds, surface temperature, and net radiation.

4. SEASONAL VARIATIONS

The seasonal cycle of the top-of-the-atmosphere insolation is the dominant driving force for the radiation budget. The difference in the seasonal cycle between warm and cool equatorial ocean regions is illustrated in Figure 7 for two ocean target areas in the latitude band (0° to 4.5°S). The monthly mean solar insolation (Figure 7a) is always high with a yearly range of 2 W/m^2 (15%). A minimum, below 400 W/^{2}, occurs in May to June while a prolonged maximum, above 420 W/m^2, occurs for September to April. The western Pacific rainy region (centered at 2.25°S latitude and 159.75°E longitude) is characterized by plentiful, high clouds and a year- round surface temperature close to 303°K (30°C). Both the net radiation and the cloud amount and altitude increase with the insolation, but the surface temperature shows a slight tendency to decrease during the monsoon peaks.

REFERENCES

Ardanuy, P. E., H. L. Kyle, and H. D. Chang, 1987: Interannual Observations of the Southern Oscillation: Results from the Nimbus-7 ERB Experiment, *Mon. Wea. Rev.*, **115**, pp. 2615-2625.

Ardanuy, P. E., C. R. Kondragunta, and H. L. Kyle, 1990: Low-Frequency Modes of the Tropical Radiation Budget, *J. Meteor. and Atmos. Physics*, **44**, 167-194.

Ardanuy, P. E., L. L. Stowe, A. Gruber, and M. Weiss, 1991: Shortwave, Longwave, and Net Cloud-Radiative Forcing as Determined From Nimbus-7 Observations, J. Geophys. Res., **96**, 18537-18549.

Arking, A., 1991: The Radiative Effects of Clouds and Their Impact on Climate, *Bull. Amer. Meteor. Soc.*, **71**, 795-813.

Dhuria, H. L. and H. L. Kyle, 1990: Cloud Types and the Tropical Earth Radiation Budget *J. Climate*, **1990**, 1409-1434.

Harrison, D. E., 1991: Equatorial Sea Surface Temperature Sensitivity to Net Surface Heat Flux: Some Ocean Circulation Model Results, *J. Climate*, **4**, 539-549.

Harrison, E. F., P. Minnis, B. R. Barkstrom, V. Ramanathan, R. D. Cess, and G. G. Gibson, 1990: Seasonal Variation of Cloud Radiative Forcing Derived from the Earth Radiation Budget Experiment, *J. Geophys. Res.*, **95**, 18,687-18,703.

Hartmann, D. L., and D. Doelling, 1991: On the Net Radiative Effectiveness of Clouds, *J. Geophys. Res.*, **96**, 869-891.

Hartmann, D. L., K. J. Kowalewsky, and M. L. Michelsen, 1991: Diurnal Variations of Outgoing Longwave Radiation and Albedo from ERBE Scanner Data, *J. Climate*, **4**, 598-617.

Hoyt, V. D., H. L. Kyle, J. R. Hickey, and R. H. Maschhoff, 1991: The Nimbus-7 Total Solar Irradiance: A New Algorithm for its Derivation, *J. Geophys. Res.*, Space Physics, (in press).

Jacobowitz, H., H. V. Soule, H. L. Kyle, F. B. House, et.al., 1984: The Earth Radiation Budget (ERB) Experiment: An Overview, *J. Geophys Res.*, **89(4)**, pp. 5021-5038.

Kyle, H. L., Ardanuy, P. E., and E. J. Hurley, 1985: The Status of the Nimbus-7 ERB Earth Radiation Budget Data Set, *Bull. Amer. Meteor. Soc.*, **66**, pp. 1378-1388.

Lewis, M. R., M. Carr, G. C. Feldman, W. Esaias, and C. McClain, 1990: Influence of Penetrating Solar Radiation on the Heat Budget of the Equatorial Pacific Ocean, *Nature*, **347**, 543-545.

Platt, C. M. R., 1981: The Effect of Cirrus of Varying Optical Depth on the Extraterrestrial Net Radiative Flux, *Quart. J. Roy. Meteor. Soc.*, **107**, 671-678.

Prabhakara, C., R. S. Fraser, G. Dalu, M. C. Wu, and R. J. Curran, 1988: Thin Cirrus Clouds: Seasonal Distribution Over Oceans Deduced from Nimbus-4 IRIS, *J. Appl. Meteor.*, **27**, 374-399.

Ramanathan, V., 1987: The Role of Earth Radiation Budget Studies in Climate and General Circulation Research, *J. Geophys. Res.*, **92(4)**, pp. 4075-4095.

Ramanathan, V. and W. Collins, 1991: Thermodynamic Regulation of Ocean Warming by Cirrus Clouds Deduced From Observations of the 1987 El Niño, *Nature*, **351**, 27-32.

Ramanathan, V., R. D. Cess, E. F. Harrison, P. Minnis, B. R. Barkstrom, E. Ahmad, and D. Hartmann, 1989: Cloud-Radiative Forcing and Climate: Results From the Earth Radiation Budget Experiment, *Science*, **243**, 57-63.

Stephens, G. L., 1990: On the Relationship Between Water Vapor Over the Oceans and Sea Surface Temperature, *J. Climate*, **3**, 634-645.

Stowe, L. L., C. G. Wellemeyer, T. F. Eck, H. Y. M. Yeh, and the Nimbus-7 Cloud Data Processing Team, 1988: Nimbus-7 Global Cloud Climatology, Part I: Algorithms and Validation, *J. Climate*, **1**, pp. 445-470.

Stowe, L. L., H. Y. M. Yeh, T. F. Eck, C. G. Wellemeyer, H. L. Kyle, and the Nimbus-7 Cloud Data Processing Team, 1989: Nimbus-7 Global Cloud Climatology, Part II: First Year Results, *J. Climate*, **2**, pp. 671-709.

Wielicki, B. A. and R. N. Green, 1989: Cloud Identification for ERBE Radiative Flux Retrieval, *J. Appl. Meteor.*, **28**, pp. 1131-1146.

FIGURE CAPTIONS

Figure 1. The annual net radiation observed by the Nimbus-7 ERB scanner for the year June 1979 to May 1980. The units are W/m^2 and the contour intervals is 20 W/m^2.

Figure 2. The annual net radiation cloud forcing observed by the Nimbus-7 ERB scanner. The contour step is 15 W/m^2. The dots indicate regions with insufficient cloud-free observations.

Figure 3. The tropical annual net radiation and its relation to the surface temperature are shown. Shadings rising from left to right indicate regions where the mean annual temperature is greater than or equal to 301°K. Shadings declining from left to right show regions where the mean temperature is less than or equal to 297°K.

Figure 4. A scatter plot of mean annual sea-surface temperature versus annual net radiation for the equatorial ocean ($\pm 4.5°$ latitude) is shown for the year June 1979 to May 1980. The data are from the Nimbus-7 ERB and cloud datasets. Each square represents one of the 111 $(500\ km)^2$ ocean target areas along the equator.

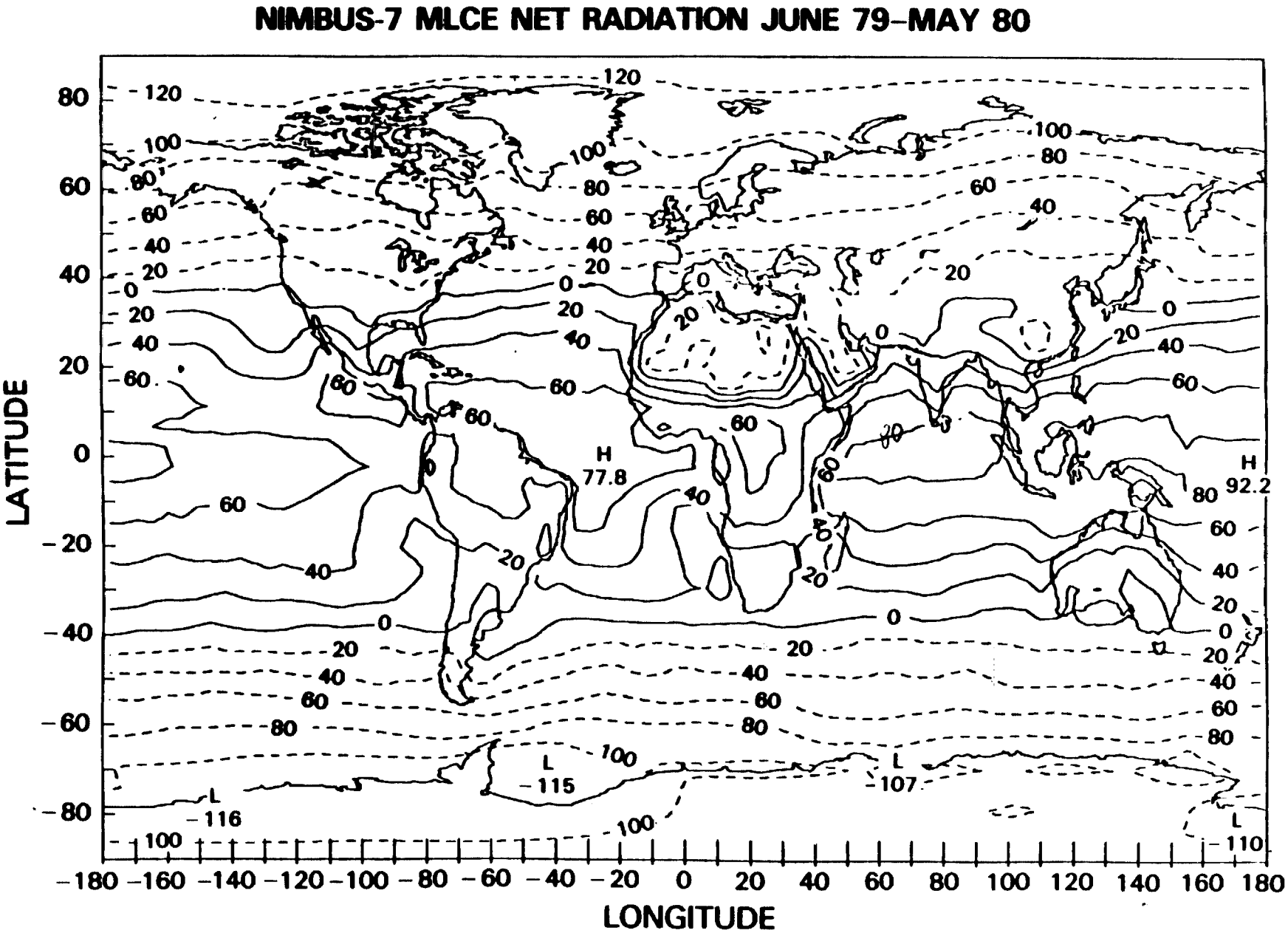
NIMBUS-7 MLCE NET RADIATION JUNE 79–MAY 80
LATITUDE
LONGITUDE
80
60
40
20
0
-20
-40
-60
-80
-180 -160 -140 -120 -100 -80 -60 -40 -20 0 20 40 60 80 100 120 140 160 180
H
77.8
H
92.2
L
-115
L
-116
L
107
L
110

Fig. 1

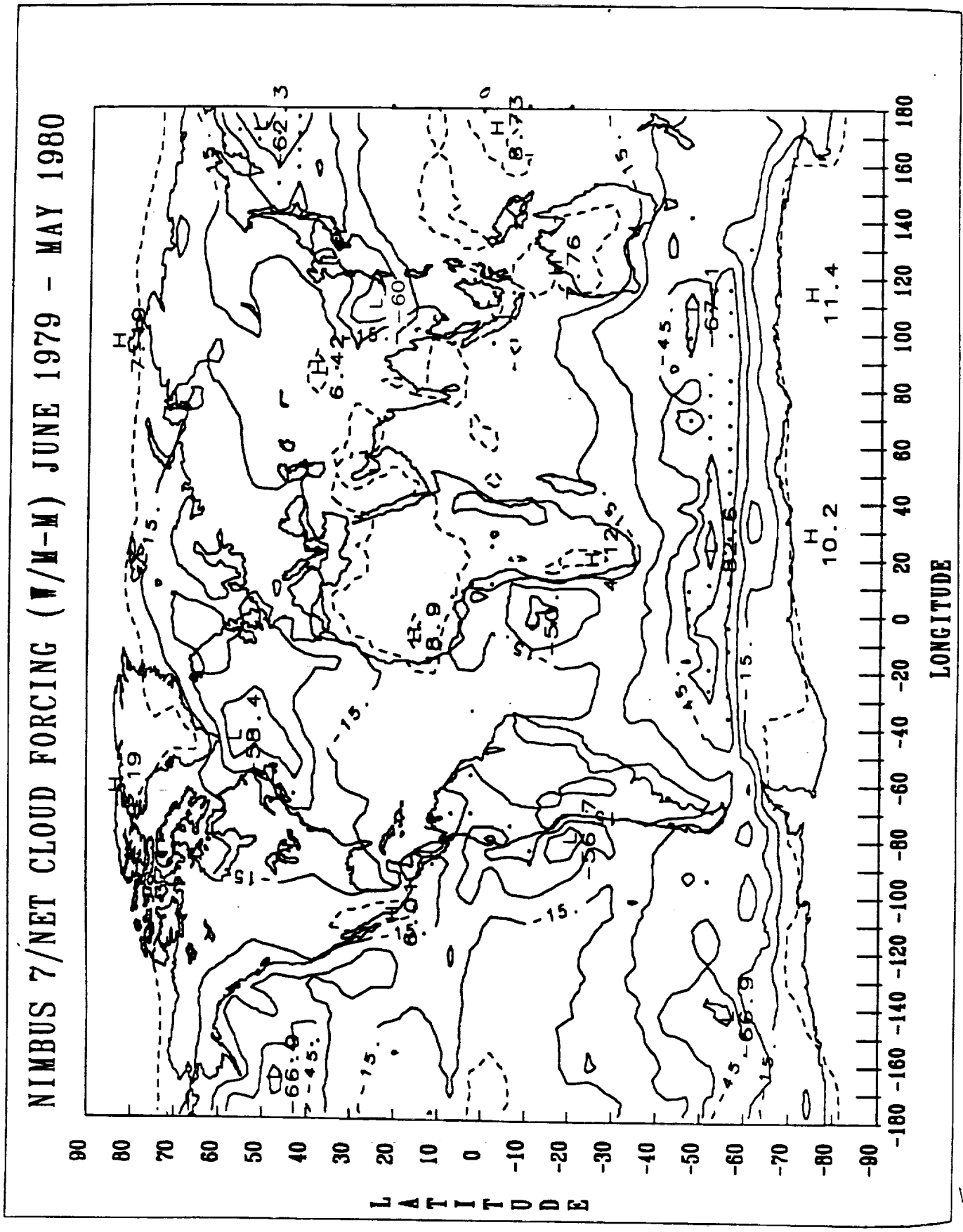
NIMBUS 7/NET CLOUD FORCING (W/M-M) JUNE 1979 - MAY 1980
LATITUDE
LONGITUDE
90 80 70 60 50 40 30 20 10 0 -10 -20 -30 -40 -50 -60 -70 -80 -90
-180 -160 -140 -120 -100 -80 -60 -40 -20 0 20 40 60 80 100 120 140 160 180

Fig 2

NET RADIATION — JUNE 1979 - MAY 1980

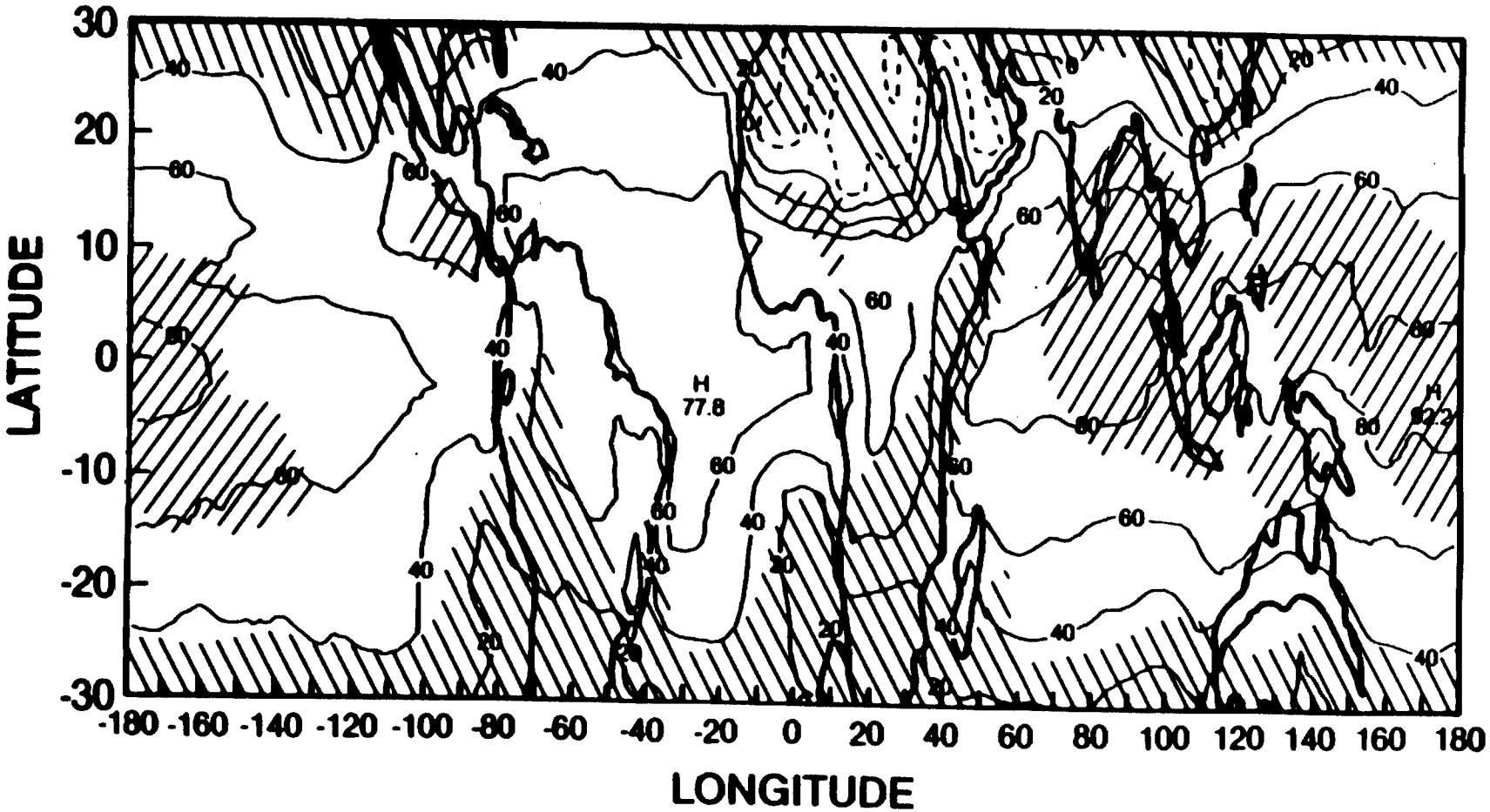

Fig. 3

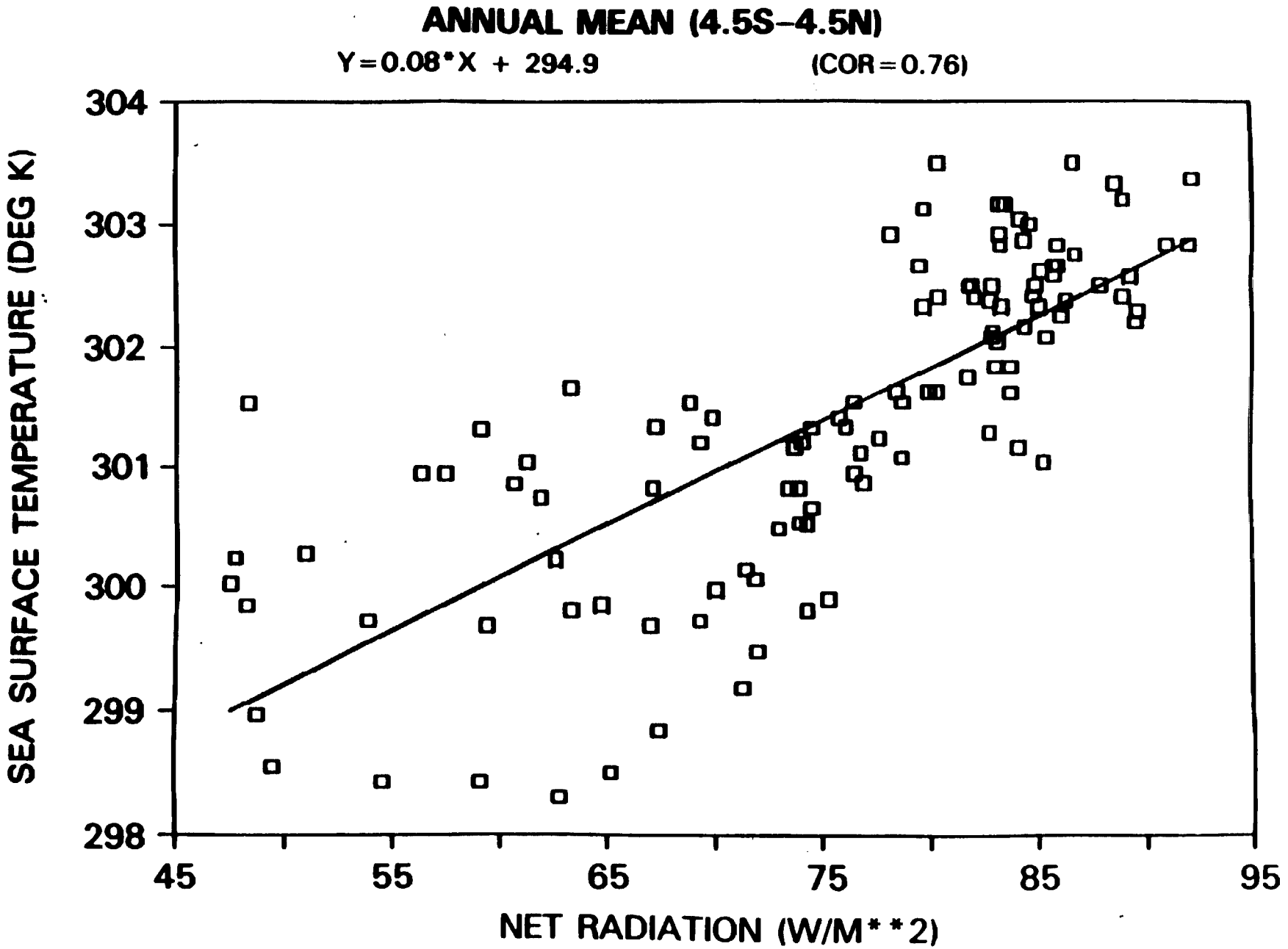
ANNUAL MEAN (4.5S–4.5N)
Y=0.08*X + 294.9
(COR=0.76)
SEA SURFACE TEMPERATURE (DEG K)
304
303
302
301
300
299
298
45
55
65
75
85
95
NET RADIATION (W/M**2)

Fig. 4